

Acoustic detection of bubbles in a pond covered by the seagrass *Cymodocea nodosa*

P. Felisberto*, J.P. Silva*, A.J. Silva*, S.M. Jesus*, I. Olivé†,
R. Santos†, H. Quental-Ferreira ‡, P. Pousão-Ferreira‡, M.E. Cunha‡

* LARSyS, University of Algarve, Campus de Gambelas, 8005-139 Faro, Portugal

† Marine Plant Ecology research group, Center of Marine Sciences of University of Algarve,
Campus de Gambelas, 8005-139 Faro, Portugal

‡ IPMA - Instituto Português do Mar e da Atmosfera, EPPO, Av. 5 de Outubro, 8700-305 Olhão, Portugal
Email: pfelis@ualg.pt

Abstract—This paper describes two experiments conducted in a pond covered by the seagrass *Cymodocea nodosa* at the Aquaculture Research Station of the Portuguese Institute for the Sea and Atmosphere in Olhão, Portugal, aiming at developing acoustic methods to assess oxygen production of seagrasses. The first experiment was carried out in July covering two days, when warm water and high photosynthetic rates give a high probability of oxygen supersaturation in water. The second experiment was carried out in late October, covering a period of 10 days, when seagrass productivity was expected to be lower than in July given the low irradiance and photoperiod. In the July experiment the high attenuation of low frequency pulses and broadband water pump noise (<20 kHz) in the afternoon is ascribed to bubbles formation during oxygen supersaturation conditions. This hypothesis is coherent with the significant increase of the backscattering level, as measured by an acoustic backscatter system operating at 0.5, 1, 2, 4 MHz. Both, the attenuation of low frequency signals and backscattering level are correlated with oxygen supersaturation in water as measured by an optode. In the October experiment, when only water pump noise was acquired, the acoustic variability that can be related to photosynthetic activity was much weaker, nevertheless the attenuation shows a diurnal pattern correlated with the dissolved oxygen. The results suggest a significant release of oxygen as bubbles during photosynthesis, and therefore the potential contribution of acoustic methods to assess oxygen production of seagrass ecosystems.

Index Terms—oxygen bubbles; seagrass meadow; oxygen production; acoustic monitoring

I. INTRODUCTION

It is well known that bubbles in water have an acoustic signature and, several methods have been developed for acoustic characterization of gas bubbles in the seawater [1]. In seagrass ecosystems, most of the oxygen produced by photosynthesis is released to the water by diffusion, but under oxygen supersaturation conditions, bubbles might be formed at the surface of leaves. Moreover, during photosynthesis the pressurization of plants aerenchyma occurs, as the oxygen produced diffuses into it [2]. Internal pressurization of 15kPa above atmospheric pressure has been reported for *Cymodocea nodosa* under the light, whereas in the dark it decreased to values below the partial pressure of air in seawater. The pressurization can also lead to bubble formation at the leaf tips, particularly if these are damaged. Aerenchyma pressurization, and particularly bubbles have an acoustic signature, therefore

acoustic based methods may be a valid tool contributing to the monitoring of seagrass ecosystems. The experiments reported in this paper, performed in the framework of SEAFOX project¹, represent a contribution for the development of such methods. The objectives were to test various acoustic methods to detect the acoustic signature of bubbles linked with photosynthesis in a *Cymodocea nodosa* ecosystem and evaluate the influence of other environmental parameters on the bubbles signature. The lessons learned from these experiments contribute for the development of a bubbles measurement system optimized for such conditions.

This paper is organized as i) introduction, ii) the principles of acoustic detection and quantification of air bubbles in water environments, iii) overview of the experimental setup, iv) data processing and initial data analysis, v) method for estimating the bubbles void fraction, and vi) conclusions.

II. PRINCIPLES OF ACOUSTIC DETECTION AND QUANTIFICATION OF GAS BUBBLES

Bubbles occur in the ocean from natural and anthropogenic origins: beneath the sea surface due to waves breaking, ship's wake, underwater vents, gas hydrates on the ocean bottom, decomposition of organic material, photosynthesis of marine plants, etc. The impact of bubbles in the acoustic signal along with methods to estimate their characteristics (sizes distributions, densities) have been reported by several authors [1], [3], [4]. In general these methods rely on the scattering and absorption properties of bubbles for signals in the frequency band of bubbles resonance, and the change of effective sound speed of the water medium for low frequency signals. Simplified relations for the characterization of underwater air bubbles in response to acoustic signals may be considered when the pressure amplitudes are small, the product of signal wavenumber (k) and bubble radius a is small ($ka < 1$), and the gas void fraction is also small. (Detailed analysis of underwater sound propagation in bubbly environments can be found in [1], [5]).

The air bubble acts as a scatterer, which is characterized by the so called scattering cross-section (the ratio between

¹funded by National Funds through Foundation for Science and Technology (FCT) under project PTDC/EEIPRO/2598/2014

the acoustic power scattered by an object to the incident wave intensity). The scattering cross-section of a bubble as the maximum at bubble resonance frequency f_0 is given approximately by [5]

$$f_0 = \frac{3.27}{a} \sqrt{1 + 0.1z} \quad (1)$$

where z is the depth. As an example the resonance frequency of a bubble of radius $100\mu m$ at $1m$ depth is $\approx 34 kHz$. When a bubble is insonified at its resonance frequency the scattering cross-section (σ_s) reaches the maximum given by

$$\sigma_s = \frac{\lambda_0^2}{\pi} = \frac{c^2}{f_0^2 \pi}$$

where c is sound speed of the water. At frequencies well below ($f \ll f_0$) and above ($f \gg f_0$) the scattering cross-section is given by

$$\sigma_s = 4\pi a^2 \left(\frac{f}{f_0} \right)^2, \quad (2)$$

and

$$\sigma_s = 4\pi a^2, \quad (3)$$

respectively. Thus, the intensity of the field scattered by the bubble is significantly lower as the frequency of the acoustic signal deviates from the bubble resonance frequency. Moreover, for frequencies well above the resonance frequency the intensity of the scattered field does not depend on the frequency. More accurate relations, which account for shear viscosity, thermal conductivity and other loss factors can be found in [1], [5], but their influence is not so important for a qualitative analysis. The major differences are a down shift of the resonance frequency and a decrease of the scattering cross-section particularly close to the resonance frequency.

In the ocean, where bubbles with various radius coexist, the intensity of the overall scattered field results from an integral value encompassing the scattering cross-sections and density of bubbles (number of bubbles per unit volume) of different sizes (see [1], [5]), that can be measured by a backscatter device [3].

On the other hand, an acoustic signal propagating through a bubbly sea water suffers attenuation due to scattering and absorption. This excess attenuation is characterized by the so called extinction cross-section (similar to the scattering cross-section). The intensity of the acoustic signal decreases exponentially with propagating distance, where the attenuation coefficient is an integral value encompassing the extinction cross-sections and density of bubbles of different sizes. Various methods have been proposed for estimating bubble populations and size distributions using short range transmission of acoustic signals [4].

A small fraction of air bubbles to the volume of water (gas void fraction) has a very significant effect on the compressibility of the mixture, given rise to a decrease of the sound speed (compared with bubble free water). The sound speed of the bubbly water is dispersive (frequency dependent), but for frequencies well below the bubbles resonance frequency,

sound speed is simply a function of the void fraction [4]. Then, the medium sound speed c_e (effective sound speed) is given by the Wood's equation [6]

$$\frac{1}{c_e^2} = \frac{(1-\chi)^2}{c_w^2} + \frac{\chi^2}{c_g^2} + \chi(1-\chi) \frac{(\rho_g c_g)^2 + (\rho_w c_w)^2}{\rho_w \rho_g (c_w c_g)^2}, \quad (4)$$

where χ is the void fraction, c_l and ρ_w , ρ_l are the sound speed of the bubbles free water and the gas, and their densities, respectively.

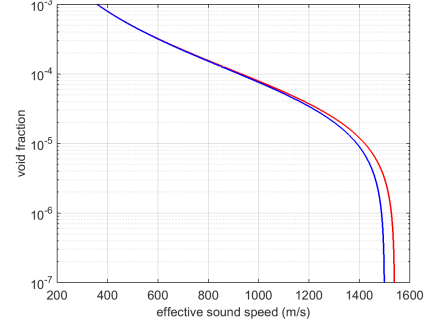


Fig. 1. Air bubbles void fraction as function of effective sound speed for different sound speed of bubbles free sea water: 1500 m/s (blue) and 1540 m/s (red)

This property has been used by several authors to determine the gas void fraction by estimating the effective sound speed from travel time measurements using close located transducer-receiver [7], [3], [4], [6]. Figure 1 shows the air void fraction as function of the effective sound speed for different sound speeds (1500 and 1540m/s) of bubble free water. It can be noticed that for large gas void fractions small differences in the gas free sound speeds can be neglected.

III. OVERVIEW OF EXPERIMENTAL SETUP

The experiments were carried out from July 25th to 27th and from October 11th to 21th, 2016 in a pond of the Aquaculture research station (EPPO) in the Ria Formosa lagoon area, Olhão, south of Portugal.



Fig. 2. EPPO areas with *Cymodocea nodosa*. The acoustic measurements were performed in pond (c). Pond (a) is connected to Ria Formosa lagoon through a tide gate. The ponds are connected by channel (b). The water pumps that feed the adjacent aquaculture tanks and station are installed in the corner labeled (c).



Fig. 3. On the left, the anchoring structure used in the July experiment with the various instruments installed; on the right, the moorings with CTD and SR-1 hydrophone used in the October experiment before deployment.

A. Site description

Figure 2 shows the ponds and the channel covered by seagrasses *Cymodocea nodosa*. The pond (a) is directly connected to the Ria Formosa through a tide gate. The acoustic measurements took place in pond (c) from where the water is pumped to various tanks in the research station. The ponds are connected by channel (b). The mean water depth at pond (c) is 1.7 m, ranging from 1.4 to 2.1 m.

The main contributions to acoustic noise in the pond is generated by the water pumps installed 30 cm from the bottom at the location labeled (c).

Cymodocea nodosa covers the whole pond bottom with few, uncovered patches. The plants had an averaged leaf length of 32.4 ± 0.5 cm. The bottom composition is unknown, but visual inspection revealed a thin sandy layer and anoxic sediments.

B. Instruments

The instruments used in the July experiment were the RBRconcerto CTD, that includes a Rinko optode to measure dissolved oxygen, the Marsensing SR-1 hydrophone to record noise and low frequency signals emitted by the Lubell LL916C sound source, and the AQUAscat 1000 backscatter system (ABS) operating at 0.5, 1, 2 and 4 MHz. The instruments were fixed to an anchoring structure (Fig. 3, left picture), deployed at about 35 m meters from the water pump area. The SR-1 hydrophone, the Lubell source and CTD were fixed at 60 cm from the bottom. The distance between the Lubell and the SR-1 was 94 cm. The ABS was installed upward looking, with the transducers at approximately 74 cm from the bottom. The Lubell transmitted every 10 min, sequences of 60, 4 period long, single-frequency pulses at 2.5, 5, 11 and 15 kHz. The SR-1 hydrophone recorded the transmitted sequences and ambient noise during 90 s every 10 min. The acoustic backscatter levels were recorded every 5 min. The CTD acquired data at a rate 1 sample/min.

During the October experiment only the SR-1 hydrophone and CTD were used, both installed in simple moorings (Fig. 3, right picture) around the same location and depth of the July experiment.

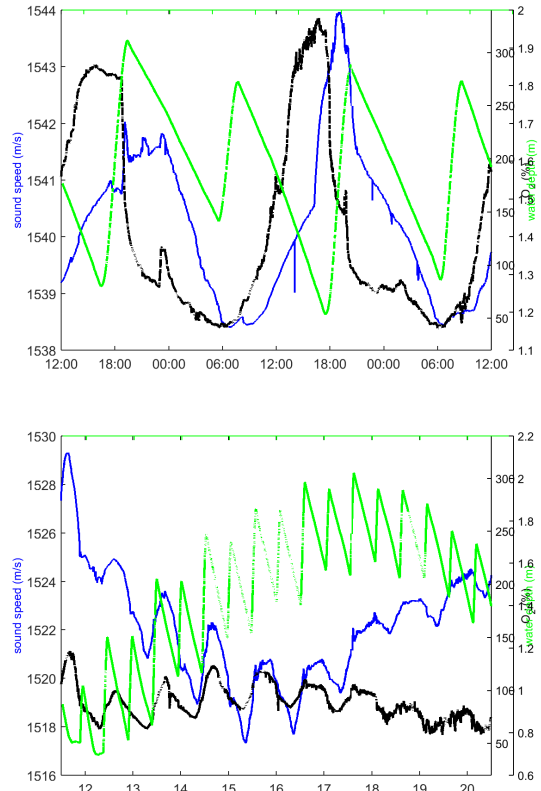


Fig. 4. CTD data measured during the July experiment (upper panel) and the October experiment (bottom panel): sound speed (blue), dissolved oxygen (black) and water depth at the pressure sensor (green)

IV. DATA PROCESSING AND PRELIMINARY ANALYSIS

In this section is presented and analyzed the acoustic data gathered in the experiments and the most relevant environmental data for acoustic data interpretation. Note that only CTD and acoustic noise data were gathered during the October experiment.

A. CTD data

The CTD acquired pressure, conductivity, temperature and dissolved oxygen saturation level at sampling frequency of 1 sample per minute during both experiments. The derived values of depth, sound speed and oxygen concentration were computed by the companion RBR software (Ruskin). The most relevant parameters for the analysis of acoustic signals (sound speed, depth and oxygen concentration) are presented in Fig. 4. Note that the sound speed given by the CTD is the bubble free value.

1) *July experiment*: The sound speed varied between 1538 and 1544 m/s showing a diurnal pattern. The CTD depth varied with tide, however instead of a (quasi) sinusoidal pattern, the water depth increases and decreases almost linearly with a higher slope (faster) during the inflow, due to the water flux control system (tide gate). The dissolved oxygen followed a diurnal pattern with a minimum at 6 am. Afterwards, rapidly

increased until 13:30. Then, until 6:30 the variation is relatively small. After 18:30, dissolved oxygen rapidly decreased. The saturation level reached very high values: approximately 290% in the 1st daily cycle and more than 300% in the 2nd daily cycle. However, under saturation occurred from 20:30 until 10:00 next day, with a minimum value below 50% of the saturation level.

2) *October experiment*: The sound speed varied between 1517 and 1529 m/s showing a diurnal pattern. Like in the July experiment, the CTD depth varied with the tide in the same way. From the CTD depth, the estimated mean water depth ranged from 1.5m to 2.25 m. This 75cm variability is important since it represents approximately 40% of the water column height, having a significant influence in acoustic signals propagation at very low frequencies. The dissolved oxygen also shows a diurnal pattern with the lowest values just before sunrise, and the highest values in the afternoon. The maximum value of dissolved oxygen is about 135%, as measured during the first day (October 11th). The aeration pump was working this day, what may affect the measurements. The values of air temperature and irradiance (not shown) that influence photosynthetic activity of plants were not maximal in the period. By the end of the day, the aeration pump was switched off. In the next three days (October 12th–14th), peaks and valleys are narrow with maximum and minimum levels at 16h30 and 6h45 respectively and an increasing trend. Afterwards, a decreasing trend of dissolved oxygen is noticed. Although, the peaks and valleys occur almost at same time of the day as in the previous period, they are wider, particularly for the peaks. It is also noticed an increasing instantaneous variability. However, measurements during last days, after October 15th, might be inaccurate due to a low battery situation. Anyway, during the whole October experiment the supersaturation conditions were weak compared with the July experiment.

B. Acoustic backscatter

In this experiment the acoustic backscatter was programmed as follows: bin size of 0.04 m, and a total of 50 bins was used, allowing a measurable distance in the water column of 2.00 meters. The burst (period during which the ABS is acquiring data) was set to 2 and half minute at a profile rate of 40 profiles per second. The profiles were averaged over a burst, to filter out high frequency fluctuations. The interval between bursts was 5 minutes.

Figure 5 shows the backscatter level measured by the 0.5 Mhz sensor. The largest background level is a line due to reflections from water-air interface (surface). The range of this reflector is highly correlated with the water depth variability due to tide, as can be seen from water depth estimated from the CTD pressure sensor (green line). The comparison suggests an offset between the estimates of water depth from CTD and backscatter. The range estimate from ABS assumes a sound speed of 1500 m/s, but the actual sound speed is about 1540 m/s. This error is less than 4% and can be neglected. Other source of errors in range estimates are discussed in [3]. However, the main source of disagreement between the two

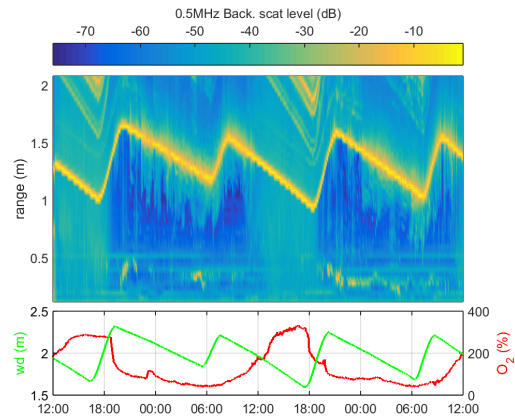


Fig. 5. Variability of the backscatter level at 0.5 MHz (bottom) during the 2 diurnal periods in July. The green and the red curve show the water depth and the dissolved oxygen, respectively.

measurements may be associated with the reference depth of the CTD. Herein was considered at the pressure sensor level, however this issue should be checked.

The backscatter beyond the surface range is due to surface reverberation. Below the surface, when the oxygen saturation level is high, the level of the scattered signal for all frequencies is high along the whole water column. Most likely this is due to bubbles released during photosynthesis and may be used for bubbles characterization (amount, distribution, size, dynamics). When the O₂ saturation level is low, one can see two continuous scatters (lines) at approximately 0.4 m and 0.5 m along time in all frequencies, but for the highest frequency (4 MHz, not shown). These scatters may be due to the anchoring structure (the beam at 4 Mhz is narrower and the sensor was the farthest from the anchoring structure). Under low oxygen saturation level, it can be seen other scatters at close ranges at various instants. These may be due to plant leaves, since during the deployment of the equipment, we have noticed leaves above the sensors depth.

C. Single-frequency pulses

The probe signals generated by the Lubell L916C source were of the the same order of magnitude of the noise generated by the water pumps. Therefore, a matched filter was applied to improve the SNR. The output of the matched filter shows a number of peaks corresponding to the arrivals from the different propagation paths between the source and the hydrophone (particularly direct, surface reflected and bottom reflected). The strength of the first peak of the matched filter output is proportional to the power of the direct arrival (assuming that the other arrivals do not overlap, or at least have relatively low amplitudes and are delayed).

For each frequency 44 out of 60 matched filter outputs were selected, neglecting these with 8 highest and 8 lowest maximum peaks. This procedure allows to discard possible outliers. Figure 6 shows the average strength of the first peak of the matched filter output at frequencies 2.5, 10 and 15 kHz along the 2 days period in July.

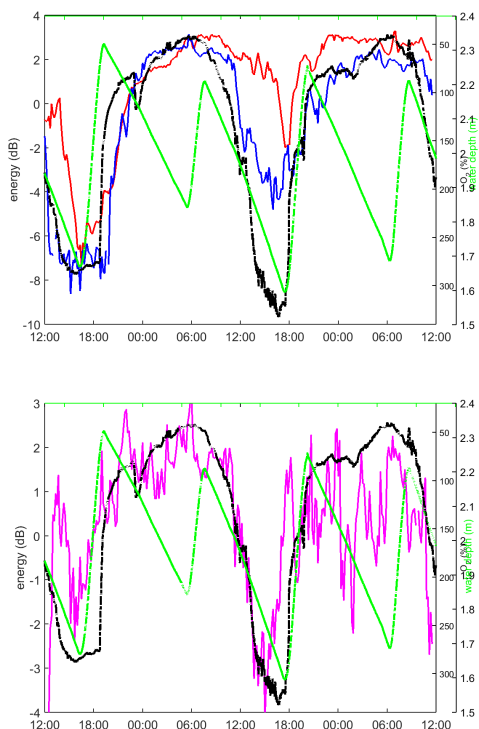


Fig. 6. Strength of the first peak of the matched filter output from pulses at 2.5 kHz (red, upper panel), 10 kHz (blue, upper panel) 15 kHz (magenta, bottom panel) from midday of 25th July to midday of 27th July. The green and black curves show the water depth and the dissolved oxygen, respectively.

The comparison between the variability of the first peak of the various probe signals presented in Fig. 6 shows a high attenuation (low power) of the signals when the oxygen saturation level is high, but with differences among frequencies and diurnal periods.

The blue line (11025 Hz signal) best fits the oxygen saturation level curve (black), however a higher attenuation would be expected during the interval of high oxygen saturation level in the second diurnal period. The red line (2490 Hz signal) is similar to the blue line, but the disagreement at the second interval of high oxygen saturation level is even worse. The magenta line (14900 Hz signal) shows high instantaneous variability, but generally follows well the oxygen saturation level curve, including the relative amplitudes of the peaks of oxygen saturation level. However during the night period of the second diurnal period, unexpected peaks of high attenuation occurs. This line related to the highest frequency shows the smallest peak to peak power variability (~ 6.5 dB), about half of the value found in the other two frequencies.

There are various factors that could explain the different behavior of the curves, particularly for the longer 2490 Hz signals there is overlap of the bottom and surface reflected arrivals and the direct arrival most of the time. The relative time of arrival depend on water depth (surface reflected) and sound speed in the water (due to bubbles concentration) and

relative attenuation. Although the most relevant contribution for the variability of the signal strength should be ascribed to attenuation due to bubbles, about 2 dB of variability were found in simulations for changes of water depth similar do those found in the experiment (not shown). If the effective sound speed of the medium falls with rising bubbles concentration then also the relative travel times change and the overlap among arrivals. In simulations this effect explained approximately 2 dB of the variability. The simulations considered only geometrical aspects and sound speed variations; scatter and absorption effects were not accounted for. The variability of the shortest signals (15 kHz) are the least affected by the water depth-sound speed variability, therefore are candidates for gas void fraction estimation (see Sec. V).

D. Ambient noise

In both the July and the October experiments, the power spectral density of noise was computed every 10 minutes from 30 s data snapshot using the Welch method with a 2048 points FFT, and 512 samples overlapping. Figure 7 shows the variability of the noise power in the July (left panel) and October (right panel) experiments, respectively. In both cases 3 bands were considered: 0–2 kHz (red curves), 2–7.25 kHz (blue curve) and 7.25–25 kHz (magenta curves). In both panels the O₂ saturation level and water depth are plotted as black and green lines respectively.

1) *July experiment.*: It can be seen that the attenuation of the ambient noise is high at daylight when the oxygen saturation level is also high, what can be ascribed to bubbles production. Although, the periods of low oxygen saturation levels have similar extent and values, the noise power is significantly lower during the second period (about 15 dB), when the aeration pumps moored at a location close to the water pumps and between them and the SR-1 hydrophone were switched on. The bubbles produced by the aeration pumps most likely attenuates the acoustic noise produced by the water pumps.

2) *October experiment.*: On October 12th at 9 am the aeration pump was switched off, giving rise to a significant increase of the noise power at the hydrophone. On October 17th at 9 am and on October 20th at 4 pm water pumps were switched off giving rise to a decrease of ambient noise. The pumps switch off events are clearly seen in the figure, where sudden changes in noise power occur at all frequencies. Apart of this, one can notice the influence of the water depth variability on the power variability of the lowest frequency band. In this experiment the supersaturation conditions are scarce and no or few bubbles might be released. Nevertheless, in the middle and high frequency bands the noise power shows a diurnal change, that may be linked with the photosynthetic activity of the plants.

V. GAS VOID FRACTION ESTIMATES

The gas void fraction was estimated during the July experiment from the single-frequency pulses at 15 kHz, assuming that the Wood's equation applies (see Sec. II). Since the

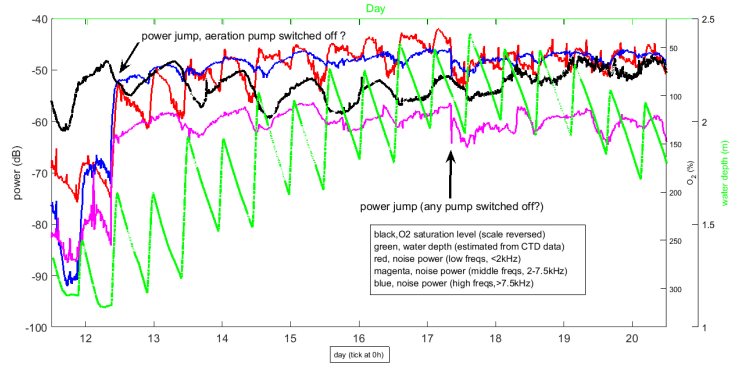
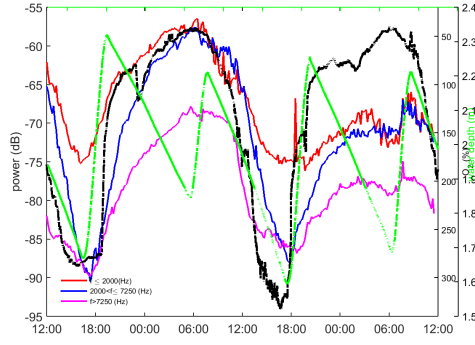


Fig. 7. Noise power estimated every 10 min in the band below 2 kHz (red), 2–7.5 kHz (blue) and above 7.5 kHz (magenta): July experiment (left panel) and October experiment (right panel). The green and black lines represent the water depth and dissolved oxygen, respectively.

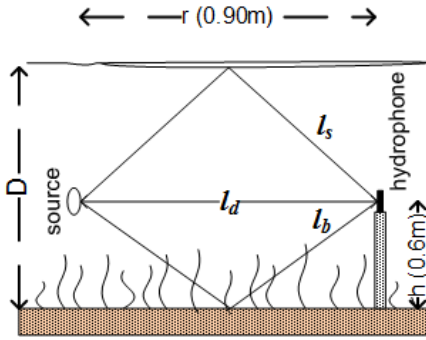


Fig. 8. Source-hydrophone geometry for single frequency pulses

synchronization between source and hydrophone was not implemented, the estimate of effective sound speed was obtained using travel time difference between the direct and bottom reflected arrivals, as follows.

Considering a constant effective water sound speed (c_e) and the geometry depicted in Fig. 8, where r is the distance between the source and the hydrophone, D is the water column height and h is the distance of source and hydrophone to the bottom, then the direct, bottom and surface reflected path lengths l_d , l_b and l_s , and respective travel times τ_d , τ_b and τ_s are given by

$$l_d = r, \quad \tau_d = l_d/c_e, \quad (5)$$

$$l_b = \sqrt{r^2 + (2h)^2}, \quad \tau_b = l_b/c_e, \quad (6)$$

$$l_s = \sqrt{r^2 + [2(D-h)]^2}, \quad \tau_s = l_s/c_e. \quad (7)$$

Taking into account the travel time difference between the direct and bottom reflect arrivals ($\Delta t_{bd} = \tau_b - \tau_d$), the effective sound speed can be estimated by

$$c_e = \frac{l_b - l_d}{\Delta t_{bd}}. \quad (8)$$

It should be noted that the path length of surface reflected arrival varies with tide. When the water level is low and the

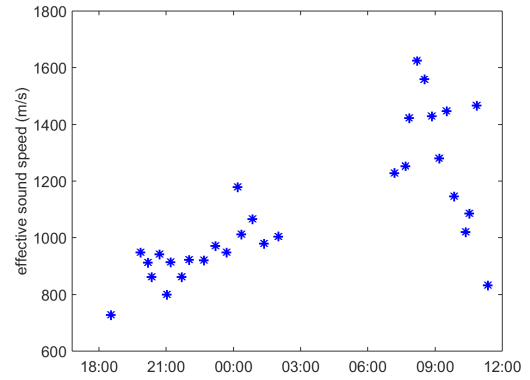


Fig. 9. Effective sound speed estimated from travel time difference between direct bottom and surface reflected echoes

effective sound speed is close to the free bubble water, the surface and bottom arrivals significantly overlap and it is impossible to determine their travel time differences. Therefore, the estimates of effective sound shown in Fig. 9 cover only two periods of the experiment. The estimates show an increase of the effective sound speed from 18:00 to 03:00, next day. This may be linked with a drop of bubbles concentration in leaves or the pressurization of the plant along the night. Early morning the trend of the effective sound speed is opposite, when a rapidly decrease of the effective sound speed can be ascribed to the increase of bubbles and pressurization due to photosynthesis. Taking into account Fig. 1, the gas void fraction reaches values of the order of 10^{-4} . Figure 10 compares the amplitude of direct and bottom surface arrivals at the instants of the effective sound speed estimates in Fig. 9. As expected the amplitude of bottom reflected are smaller than the direct arrivals. But, whereas the fluctuation of the amplitude of direct arrivals does not show a visible trend, the amplitude of bottom reflected arrivals increases along the night (attenuation decreases) and decreases along the morning period. Bearing in mind that path of direct arrivals are above

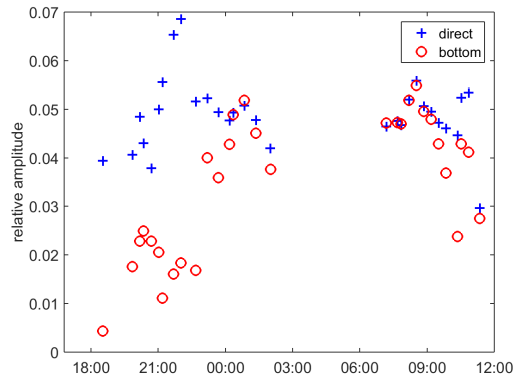


Fig. 10. Amplitude of direct and bottom reflected arrivals for the instants in Fig. 9

the plants and bottom reflected arrivals travel through the plants, it suggests important bubbles/pressurization dynamic in the plant layer during the night. The errors associated with these estimates are expected large, because of the low SNR and the environmental/geometrical conditions of the setup discussed above, nevertheless the overall trends are clear seen in Fig. 9 and 10.

VI. CONCLUSIONS

The results suggest the significant formation of oxygen bubbles during photosynthesis in this ecosystem. During the July experiment, the acoustic backscatter significantly increased during daylight in oxygen supersaturation conditions, as measured by the optodes. Simultaneously, transmitted single-frequency pulses at low frequencies were significantly attenuated. The behavior of high frequency backscatter and low frequency pulses can be ascribed to bubbles formation due to photosynthesis. The increased attenuation during photosynthetic production of oxygen was also observed in the noise power, particularly in the July experiment, but also during the October experiment under weaker oxygen production and supersaturation conditions. It was also shown that water depth variability affects significantly the acoustic propagation in the pond and must be considered in bubbles quantification. Using a method to estimate the effective sound speed from the travel time difference between direct and bottom surface reflection and assuming that the Wood's equation applies, an estimate of the gas void fraction as high as 10^{-4} was obtained.

These preliminary experiments indicate significant release of bubbles by marine plants associated to photosynthesis, and gives insights for the setup of next experiments in order to attain an accurate quantification of bubbles production.

ACKNOWLEDGMENT

This work was funded by National Funds through Foundation for Science and Technology (FCT) under project PTDC/EEIPRO/2598/2014 (SEAOX).

REFERENCES

- [1] H. Medwin and C. S. Clay, "Chapter 8 - bubbles," in *Fundamentals of Acoustical Oceanography*, H. Medwin and C. S. Clay, Eds. San Diego: Academic Press, 1998, pp. 287 – 347.
- [2] J. Borum, K. Sand-Jensen, T. Binzer, O. Pedersen, and T. M. Greve, *Oxygen Movement in Seagrasses*. Springer, 2006, pp. 255–270.
- [3] S. Vagle and D. M. Farmer, "A comparison of four methods for bubble size and void fraction measurements," *IEEE journal of oceanic engineering*, vol. 23, no. 3, pp. 211–222, 1998.
- [4] E. J. Terrill and W. K. Melville, "A broadband acoustic technique for measuring bubble size distributions: Laboratory and shallow water measurements," *Journal of Atmospheric and Oceanic Technology*, vol. 17, no. 2, pp. 220–239, 2000.
- [5] L. Brekhovskikh and Y. Lysanov, "Chapter 11 - scattering and absorption of sound by gas bubbles in water," in *Fundamentals of Ocean Acoustics*. New York: Springer-Verlag, 2003, pp. 250 – 264.
- [6] P. S. Wilson and K. H. Dunton, "Laboratory investigation of the acoustic response of seagrass tissue in the frequency band 0.5–2.5 khz," *The Journal of the Acoustical Society of America*, vol. 125, no. 4, pp. 1951–1959, 2009.
- [7] E. Lamarre and W. K. Melville, "Instrumentation for the measurement of sound speed near the ocean surface," *Journal of Atmospheric and Oceanic Technology*, vol. 12, no. 2, pp. 317–329, 1995.